Seasonal cycle of circulation in the Antarctic Peninsula and the off-shelf transport of shelf waters into Southern Drake Passage and Scotia Sea

Mingshun Jiang[*1], Matthew A. Charette[2], Christopher I. Measures[3], Yiwu Zhu[1], and Meng Zhou[1]

[1]Department of Environmental, Earth and Ocean Sciences, University of Massachusetts Boston
100 Morrissey Blvd., Boston, MA 02125

[2]Department of Marine Chemistry and Biogeochemistry, Woods Hole Oceanographic Institution, Woods Hole, MA 02543

[3]Department of Oceanography, University of Hawaii, Honolulu, HI 96822

To be submitted to Deep-Sea Research II

1st revision, October 19, 2012

2nd revision, January 23, 2013

[*] Corresponding author, email: mingshun.jiang@umb.edu

Abstract

The seasonal cycle of circulation and transport in the Antarctic Peninsula shelf region is investigated using a high-resolution (~2km) regional model based on the Regional Oceanic Modeling System (ROMS). The model also includes a naturally occurring tracer with a strong source over the shelf (radium isotope ^{228}Ra, $t_{1/2}$=5.8 year) to investigate the sediment Fe input and its transport. The model is spun up for three years using climatological boundary and surface forcing and then run for the 2004-2006 period using realistic forcing. Model results suggest a persistent and coherent circulation system throughout the year consisting of several major components that converge water masses from various sources toward Elephant Island. These currents are largely in geostrophic balance, driven by surface winds, topographic steering, and large-scale forcing. Strong off-shelf transport of the Fe-rich shelf waters takes place over the northeastern shelf/slope of Elephant Island, driven by a combination of topographic steering, extension of shelf currents, and strong horizontal mixing between the ACC and shelf waters. These results are generally consistent with recent and historical observational studies. Both the shelf circulation and off-shelf transport show a significant seasonality, mainly due to the seasonal changes of surface winds and large-scale circulation. Modeled and observed distributions of ^{228}Ra suggest that a majority of Fe-rich upper layer waters exported off-shelf around Elephant Island are carried by the shelfbreak current and the Bransfield Strait Current from the shallow sills between Gerlache Strait and Livingston Island, and northern shelf of the South Shetland Islands, where strong winter mixing supplies much of the sediment derived nutrients (including Fe) input to the surface layer.

Key words: Model, circulation, Antarctic Peninsula, Antarctic Circumpolar Current, Elephant Island, off-shelf transport, Fe, Drake Passage, southern Scotia Sea

1. Introduction

The Antarctic Peninsula (AP) is located at the northernmost point of the Antarctic continent, facing South America across the Drake Passage (Figure 1). The AP shelf region supports a productive marine ecosystem, yet it is experiencing the strongest impacts of climate change among the regions of Antarctic continent. For example, winter air temperatures in the western Antarctic Peninsula (WAP) have increased about 6ºC in the last half century (Vaughan et al., 2003). Such a warming trend, along with other dramatic changes in environmental conditions, has imposed unprecedented pressure on the ecosystem (Ducklow et al., 2007).

The AP shelf area is also important to the productivity in the southern Drake Passage and the Scotia Sea. Shelf waters in the AP area are rich in dissolved iron, the limiting micro-nutrient for phytoplankton growth in the Southern Ocean (Martin et al., 1990). Recent studies have suggested that as the Antarctic Circumpolar Current (ACC) passes through the Shackelton Fracture Gap (SFG), it impinges upon the shelf around Elephant Island (EI) and interacts with the shelf currents to drive strong off-shelf transport of iron-rich shelf waters (Zhou et al., 2010, this volume). This iron flux is likely important to the massive and persistent phytoplankton blooms in the southern Scotia Sea observed from both satellite images (Kahru et al., 2007) and in-situ measurements (e.g. Holm-Hansen et al., 2004; Korb et al., 2010).

Recent studies have suggested a coherent circulation pattern in the AP shelf region. Along the northwest Weddell shelf, both the Antarctic Coastal Current (CC) and Antarctic Slope Current (ASC) flow northeastward with a typical velocity of 10 cm/sec (Muench and Gordon, 1995; Thompson and Heywood, 2008). Thompson et al. (2009) suggested that a majority of the ASC follows the continental slope moving along the Weddell slope, and some of which may cross the Philip Ridge toward the northeast EI shelf. A portion of the ASC may join the CC to

turn southward into the BS after passing Joinville Ridge (von Gyldenfeldt et al., 2002; Thompson and Heywood, 2008; Thompson et al., 2009).

Within BS, the combined southwestward current, referred to as the southern BS Current (SBSC) hereafter, meets the relatively warm and fresh waters from the WAP through the Gerlache Strait Current (GSC) at the western end of the strait (Niiler et al., 1991; Zhou et al., 2002, 2006). Together they feed into the eastward flowing BS Current (BSC), which is a strong and narrow (4-6 km wide) jet with a 50 cm/sec velocity flowing along the steep northern slope of BS (Zhou et al., 2006). Zhou et al. (2006) suggested that the BSC is mainly driven by beta-effects and the wind curl over the strait, a mechanism similar to the formation of western boundary currents in major ocean basins.

North of the South Shetland Islands (SSIs), the Southern Boundary of the ACC (SBACC) follows the continental slope eastward passing through the SFG, and once through the gap, may impinge up the shelf east of EI (Zhou et al., 2010). Before passing the gap, however, a small portion of the SBACC may detour southward and intrude into the eastern basin of BS through the passage between King George Island (KGI) and EI. The SBACC intruding flow, BSC, and the ASC crossover flow appear to all converge in the area east of EI interacting with the impinging ACC, leading to strong mixing between these flows and a strong off-shelf transport of shelf waters.

There is limited information about the seasonal cycle of the circulation in this area. Most of the studies noted above took place in austral fall and summer or reflected an annual mean such as those that employed drifters (Zhou et al., 2006; Thompson et al., 2009). In particular, there is little information about the winter circulation within BS and around EI. One exception to this is the mooring study by von Gyldenfeldt et al. (2002), which revealed remarkably consistent

currents over the Joinville Ridge for a period of about two years. Winter circulation can be important to overall shelf Fe transport because deep winter mixing may entrain a large amount of dissolved iron into the surface layer for off-shelf transport. Most of this iron may be transported toward Elephant Island given the low winter biological removal rates.

Although previous studies have demonstrated the existence of strong off-shelf transport of iron-rich shelf waters around EI area, several important aspects of the transport remain unclear. These include detailed knowledge of the iron sources and fluxes, their pathways to reach the EI area and beyond, and the dynamic mechanisms driving the off-shelf transport. Zhou et al. (2010) suggested that the off-shelf transport is due to Rossby adjustment when the southern branch of ACC passing through the SFG climbs the shelf/slope. Meso-scale eddies may form as the jet becomes unstable and may subsequently contribute to the off-shelf flux. In addition, the interactions of several different water masses may induce complex mixing between shelf waters and ACC waters. We will refer this area as the EI Transport and Mixing Zone (EITMZ) hereafter.

It is generally believed that the Fe in the shelf waters around Elephant Island is supplied from sediments on the AP shelf (Measures et al., this issue, Hatta et al., this issue). However, the precise sources of Fe and their transport pathways to reach the EI shelf region remain unclear. In this manuscript, we incorporate into the model a naturally occurring tracer of sediment-water interaction (radium isotope ^{228}Ra, $t_{1/2}$=5.8 year), which has been used in the Southern Ocean to quantify sediment-derived Fe input and to investigate its transport and dispersion (Charette et al. 2007; Dulaiova et al. 2009).

In this manuscript, we present a numerical model developed for the AP shelf and surrounding areas, and then use the model to investigate the circulation pattern, its seasonal variability, and

1 the dominant underlying processes. In section 2, a brief description of the model and data used
2 for this study is presented. In section 3, we evaluate the model's ability to capture key physical
3 features by comparing the model results with available data. Model results of the circulation in
4 the AP shelf region and its seasonal variability are presented as well. In section 4, we discuss the
5 key physical processes that control the circulation and its variability, the dynamic processes
6 associated with the off-shelf transport, and the sources and pathways of Fe-rich shelf waters
7 reaching the Elephant Island shelf and beyond. A brief summary is presented in section 5.
8

2. Model and data

2.1. Model

A high-resolution regional circulation model has been developed for the Antarctic Peninsula, Drake Passage, Scotia Sea, northern Weddell Sea, and South Georgia with a horizontal resolution of 2–15 km (Figure 1). The numerical simulations are intended to resolve circulation around the AP shelf, and therefore the highest model resolution (~2km) is centered over the AP shelf and slope. The model is based on the Regional Oceanic Modeling System (ROMS), which is a terrain-following S-coordinate modeling system (Shchepetkin and McWilliams, 2005). There are 40 vertical layers, allowing the distribution of vertical grid thickness to vary from a nearly uniform distribution in shallow areas to one more focused on the surface layer in deep areas. A third-order upstream scheme is used for horizontal advection in the momentum equation, while a fourth-order leap-frog scheme is used for vertical advection. A multi-dimensional positive definite advection transport algorithm is used for the computation of tracer advection to avoid spurious negative tracer concentrations (Smolarkiewicz, 1984). A Smagorinsky-type of mixing is used for horizontal viscosity and diffusivity (Smagorinsky, 1963), in which the viscosity is computed from current shear and grid size, and diffusivity is set to be $1/10^{th}$ of the viscosity. In the AP shelf region, the viscosity and diffusivity are approximately 10 m^2/sec and 1 m^2/sec, respectively. A second-order algorithm is used to compute the pressure-gradient term in order to reduce the so-called sigma-coordinate truncation error (Shchepetkin and McWilliams, 2003). Vertical mixing is computed using the non-local K-profile vertical mixing scheme (KPP) (Large et al., 1994).

The model is initialized with the climatological temperature and salinity from the World Ocean Atlas 2009 (WOA09) (Antonov et al., 2010; Locarnii et al., 2010), spun-up for three years

with monthly climatological forcing, and then run for the period 2004-2006 using monthly forcing for each particular year. The model surface forcing parameters include sea surface temperature (SST), sea surface salinity (SSS), winds, solar radiation, relative humidity, precipitation, air pressure, and air-temperature. For the climatological simulation (spin-up), SST and SSS are derived from the Comprehensive Ocean Atmospheric Data Set (COADS) (Da Silva et al., 1994), and other parameters are derived from the long-term (1980-2010) monthly means of National Centers for Environmental Prediction (NCEP) re-analysis 2.0 products (Kalnay et al., 1996). The relative humidity and precipitation are from the long-term (1987-2006) monthly mean of Hamburg Ocean Atmosphere Parameters and Fluxes from Satellite Data (HOAPS) (Andersson et al., 2010). For the 2004-2006 simulation, SST and SSS are derived from the 1/4° global Ocean Circulation and Climate Advanced Model (OCCAM) (Webb et al., 1998), and meteorological parameters are again from NCEP and HOAPS products for the specific period.

A bulk formulation from NCAR Community Climate System Model (CCSM) is used to compute the wind stresses and heat fluxes using surface winds and other meteorological parameters (Collins et al., 2006). To reduce uncertainty due to computed surface heat and salt fluxes, surface temperature and salinity are restored to prescribed SST and SSS with a variable time-scale depending on ocean heat sensitivity for temperature and a fixed 30-day time-scale for salinity, respectively. The correction terms are applied to the model top layer. However, in effect heat or salt changes are mixed over the entire surface mixed layer, which is generally deeper than the model top layer. Therefore, the resulting response time-scale for the mixed layer is much longer than the nudging time-scale. On average, the effective time-scales for both temperature and salinity restoration for the surface mixed layer are about 20 days in summer and 100 days in winter, which allows dynamic intrinsic variability to develop properly. The model also has a

fully integrated sea-ice sub-model using a combination of the elastic-viscous-plastic (EVP) rheology (Hunke and Dukowiz, 1997; Hunke, 2001) and simple one-layer ice and snow thermodynamics with a molecular sub-layer under the ice (Mellor and Kantha, 1998).

The model open boundary conditions include temperature, salinity, and mean sea level, and diagnostic geostrophic currents with these parameters. For the climatological simulation, boundary temperature and salinity are from WOA09; for the 2004-2006 simulation, they are from the OCCAM ¼° model output. Sea level is derived from the monthly mean dynamic height provided by AVISO (http://www.aviso.oceanobs.com/) augmented with the OCCAM sea level because AVISO data does not cover the southern portion of our model domain.

The model includes an additional tracer component to simulate short-lived or nearly inert tracers such as the radium isotopes ^{224}Ra ($t_{1/2}$=3.66 day) and ^{228}Ra ($t_{1/2}$=5.75 year). These tracers are initialized with zero values, and a uniform sediment flux (arbitrary units) is applied to the bottom layer for the AP shelf area only, to provide continuous input. Boundary values of these tracers are set to zero as we are mainly concerned with the sources and fates of sediment input from the AP shelf region. In this manuscript, we only will use only ^{228}Ra and treat it as an inert tracer given its long half-life relative to the dynamic upper ocean mixing processes taking place in this region. The purpose of including a Ra tracer is to understand the vertical mixing and horizontal pathways of sedimentary Fe input, and therefore no real sediment flux rate is necessary. In the figures presented below, however, modeled values are linearly multiplied by a constant factor so that the modeled values have a comparable range with observations from ^{228}Ra (Dulaivoa et al. 2009).

2.2. Data

In order to gauge the model performance, model results have been compared with available climatological and cruise survey data. In this manuscript, we report three types of comparisons: (1) the large-scale mean circulation pattern with satellite measured sea surface dynamic height (SSH), (2) hydrographic properties with in-situ measurements of temperature, salinity, and (3) modeled ^{228}Ra with in-situ measurements. The SSH was from the AVISO satellite altimetry products, which are derived by merging measurements from several satellites (http://www.aviso.oceanobs.com/). The temperature and salinity data were collected during the February 12-March 24 2004 (LMG0402) and July 3-August 15 2006 (NBP0606) cruises by standard CTD casts (Zhou et al., 2010; Zhou et al, this volume). The LMG0402 cruise covered an area about 200 km x 200 km northeast of Elephant Island and the NBP0606 ran several transects through the BS and around EI. In addition, surface salinity and radium isotope data were collected during the January 14-February 8 2006 Antarctic Marine Living Resources (AMLR) summer cruise (Dulaiova et al., 2009). More details on the sampling and data processing for LMG0402, NBP0606 and AMLR 2006 cruises can be found in Zhou et al. (2010), Zhou et al. (this volume) and Dulaiova et al. (2009), respectively.

3. Results

3.1. Model skills

Modeled sea level and surface currents in the Drake Passage and Scotia Sea region are compared with the long-term mean of AVISO SSH in Figure 2. Both the modeled and observed sea levels suggest that a strong Polar Front (PF) (contour -60 cm for the data and 0.6 m for the model) resides in the northern part of the Drake Passage. A relatively weaker but broader southern ACC front (SACCF) runs through the southern Drake Passage nearly parallel to the PF. A portion of the SACCF turns southward before encountering the Shackelton Traverse Ridge (STR), and then returns northward along the eastern side of the ridge. The southern boundary of ACC (SBACC) follows the Antarctic continental slope before passing through the SFG. However, it meanders dramatically after passing the SFG and a significant portion separates from the slope moving into southern Scotia Sea. This pattern is generally consistent with previous studies based on long-term hydrographic data, current measurements, and drifter trajectories (Orsi et al., 1995; Cunningham et al., 2003; Zhou et al., 2010).

Model results also suggest that the SACCF is relatively weak with currents around 20 cm/sec west of the STR, whereas along the SSIs shelf slope, the SBACC currents are about 30-40 cm/sec. The convergence of these two currents in the SFG results in currents in the SFG of >70 cm/sec (Zhou et al., 2010). After passing through the gap, the combined flow of SACCF and SBACC splits into three branches: the first one moves northward along the eastern side of the ridge to join the main ACC, the second flows through the middle of the Ona Basin into the ACC, and the third branch meanders but can be in close contact with the Antarctic shelf slope. It is worth noting that both modeled fields and AVISO SSH show three northward meanderings of SBACC in association with the topographic features: 1) the junction between the SFG and EI at

around 57ºW, 2) over the Shackelton Bank (SB) around 54ºW, and 3) Terror Rise (TR) around 51ºW. On the last meandering, the mixed cold shelf waters are pushed more than 200km into the southern Scotia Sea.

Modeled temperature and salinity in February 2004 around the EI area generally agree well with the observations (Figure 3), although modeled salinity in the off-shelf plume is lower than in the observations. Both modeled and observed temperature and salinity suggest that after passing through the SFG, the ACC waters turn sharply northward into the Ona Basin. At the same time, a significant amount of shelf water is entrained into the off-shelf transport as indicated by the cold and high salinity plume, which is present from the surface to deeper than 200m (Zhou et al., 2010).

To illustrate the model performance in winter, modeled temperature and salinity in August 2006 are compared with measurements during the NBP0606 cruise (July-August 2006) along the BS transect through the middle of the Bransfield Strait (Figure 4). Both modeled and observed results show strong gradients of temperature and salinity from north to south, and a cool but relatively fresh surface layer on top of the warm and salty deep waters in the central basin. Along both the northern and southern shelf/slope regions, observations show that the water column is well mixed down to ~500m, whereas the modeled mixed layer is much shallower, at about 100m. This is likely due to weaker sea ice formation in the model (not shown) as a result of the use of the monthly forcing, which smoothes out the effects from major storm events. Model results also show that the cold and salty waters in the southern BS shelf are associated with weak southwestward currents centered on the shelf margin. In contrast, a strong eastward narrow BSC can be found along the steep northern slope, in association with relatively fresh but warm water. The modeled speed of the BSC is about 20-30 cm/sec throughout the year, which is generally

slower than that the >50 cm/sec reported by Zhou et al. (2002, 2006) based on an analysis of surface drifter data and measurements with an Acoustic Doppler Current Profiler (ADCP).

The degree of agreement between model results and observations can be further quantified through a simple point-to-point correlation analysis, which shows significant correlations between modeled and observed temperature and salinity during summer 2004 and winter 2006 (Figure 5). However, there are also obvious discrepancies. In particular, the model appears to have under-predicted the surface salinity over the EI slope region in the summer 2004, which is about 0.1-0.3 psu lower than that observed during the LMG0402 cruise (Figure 5c). In addition, the correlation is somewhat biased by the extreme values during summer and winter cases (Figure 5b-d). However, after removing those extreme data points for temperature in the winter 2006 (modeled $T > 1^{o}$C), salinity in summer 2004 (modeled $S > 34$ psu), and salinity for winter 2006 (modeled $S<34$ psu), the modeled values are still significantly correlated with data with $r=0.2$ ($p<0.05$), $r=0.42$ ($p<0.01$), and $r<0.46$ ($p<0.01$), respectively.

A similar comparison for temperature and salinity at 400m is shown in Figure 6. Modeled temperature northeast of EI in summer 2004 remains significantly correlated with data ($r=0.75$, $p<0.01$) (Figure 6a). The modeled temperatures, however, cluster around two values, whereas observed temperatures cover the entire range (-1 ~ 2 ^{o}C). This is in contrast to the winter 2006 case, in which modeled and observed temperatures are nearly linearly correlated ($r=0.84$, $p<0.01$) (Figure 6b). The modeled and observed salinity at 400 m show much weaker yet significant correlations with modeled salinity having narrower ranges during both summer 2004 and winter 2006 (Figure 6c, d).

We also compare modeled surface salinity and inert tracer concentration in January 2006 with the observed salinity and ^{228}Ra during the AMLR summer (January 14-February 8) 2006

cruise (Figure 7). Both modeled and observed salinity show a strong NW-SE gradient between relatively fresh ACC waters in the southern Drake Passage and the high salinity Weddell waters in the southern BS and northwestern Weddell shelf (Figure 7a, c). The modeled salinity of shelf waters surrounding SSIs falls between that of the ACC waters and the Weddell waters. Model results also show that a portion of high salinity Weddell slope water is transported across the south Scotia Ridge by the ASC passing Clarence Island (CI) into the EITMZ, consistent with previous studies (Thompson and Heywood, 2008; Thompson et al., 2009). A significant correlation is found between the modeled and observed salinities (r=0.6, p<0.01), although again a weaker salinity gradient across the shelf is indicated in the model than seen in the observations.

Both modeled and observed ^{228}Ra show high surface concentrations surrounding the SSIs, although observed ^{228}Ra is much more patchy (Figure 7b, d). Model results also show high ^{228}Ra concentration in the southwestern end of BS, where there were no sampling stations. Model results suggest that the shelf waters with high ^{228}Ra concentration at the western end of BS are transported northward through the channel between Smith Island and Livingston Island to the shelf margin, and then northeastward along the shelf margin toward EI. On approaching EI, a majority of the high ^{228}Ra waters pass through the northern slope of EI, whereas the remaining portion passes through the channel between EI and CI. The model predicts lower surface ^{228}Ra concentrations than those observed in the eastern basin of BS (Figure 7d). The observed ^{228}Ra distribution also indicates that sediment input may spread through the middle of the eastern basin toward EI. Overall, the modeled ^{228}Ra distribution is significantly correlated with the observed values (r=0.3, p<0.01).

3.2. Hydrography and circulation patterns in the AP shelf/slope region

Model results indicate a coherent spatial pattern of water masses in the AP shelf region (Figures 3, 4 and 7). Relatively fresh waters occupy the western AP with surface salinity below 33.4 psu in summer and about 33.7 psu in winter. A mixture of salty/warm ACC waters and the fresh/cold waters from the WAP is found along the northern slope of the SSIs shelf. In contrast, waters over the inner shelf area of the SSIs have a relatively high salinity. Within the Bransfield Strait, relatively fresh and warm waters occupy the narrow northern slope area and western end of the strait with temperatures around 0 °C in winter and 2-3 °C in summer, and salinities of ~34.0 psu in winter and ~33.8 psu in summer. The cold and salty Weddell waters occupy most of the Bransfield Strait with temperatures around -2°C in winter and 1°C in summer, and salinities of ~34.2 psu in summer and > 34.4 psu in winter. The summer pattern is generally consistent with the AMLR long-term survey results (Amos, 2001; Brandon et al., 2004).

Model results also show a coherent and persistent circulation pattern in the AP shelf region throughout the year (Figure 8). Along the northwestern Weddell shelf, model results show that a weak but broad CC (10 cm/sec), flows northeastward and turns around at the tip of the peninsula into Bransfield Strait, similar to the results of previous studies (von Gyldenfelt et al., 2002). The ASC associated with Antarctic Slope Front (ASF) is positioned between the 500-800 m isobaths, with currents of ~10 cm/sec flowing along the slope toward the northeast as well (Heywood et al. 2004; Thompson and Heywood, 2008; Thompson et al. 2009). A portion of the ASC turns southward into Bransfield Strait at the trough between the eastern basin of the strait and Powell Basin. The main ASC continues along the slope of Powell Basin with a small portion crossing the Philip Ridge to join the mixed ACC-shelf waters in EITMZ (see section 3.3) and the rest merging to the Weddell Front (WF) (Heywood et al. 2004; Thompson and Heywood, 2008;

Thompson et al. 2009). The Weddell Front loops around the South Orkney Plateau, and exits the Weddell Sea in the eastern side of the plateau to join the SBACC (not shown).

The CC and the returning portion of ASC combine to become the southern Bransfield Strait current (SBSC), which is a sluggish current and tends to leak into the deep basins. The SBSC returns at the western end of BS, joined by the eastward flowing Gerlache Strait Current (GLC) to form the narrow BSC jet (about 5-10 km width) along the northern BS slope. The modeled BSC speed is about 20-30 cm/sec, which is lower than the previous estimate of >50 cm/sec based on drifters and ADCP measurements (Zhou et al. 2002, 2006; Thompson et al. 2009). The BSC largely exits through the gap between EI and CI to join the EITMZ.

Along the northern SSIs slope, the SBACC flows toward the SFG with a speed of 20-40 cm/sec as noted above (Figure 8). Model results suggest that a shelfbreak current also exists along the SSIs shelfbreak, but is mainly limited to the top 200m (not shown). The shelfbreak current transport waters from the WAP shelf to join the eastward SBACC. On approaching the EI-STR segment, a portion of ACC-shelf waters may intrude into Bransfield Strait to join the BSC toward EI. Over the inner shelf of SSIs, currents are weak and generally southwestward (see section 3.4).

3.3. Off-shelf transport around Elephant Island

Model results indicate intensive off-shelf transport over the shelf/slope northeast of EI, represented as a series of meanderings of the SBACC away from the South Scotia Ridge, along with an off-shelf excursion (northeastward) of shelf waters and subsequent mixing with ACC waters (Figures 2, 3 and 8). The result is an expanding plume of mixed shelf-ACC waters being transported toward the southern Scotia Sea. As noted above, three separation points of SBACC from the shelf/slope can be identified: 1) the northern slope of EI around 57ºW, 2) the western

flank of the Shackleton Bank around 54ºW, and 3) the southwestern end of Terror Rise around 51.5ºW. Similar separation points are also present in the mean currents derived from drifter trajectories (Zhou et al. 2010) and the SSH map (Figure 2). At the bottom of the northern EI slope, the SACCF passes through the SFG and a portion makes a sharp north turn following the eastern side of the STR. The meandering of the SBACC and the SACCF combined transport a significant amount of mixed water northward. At the second separation point, however, modeled currents indicate that a majority of the northward transported waters returns to intercept the shelf/slope further east. In contrast, the off-shelf meandering at the third point produces a broad plume of mixed waters that spreads much further offshore and downstream.

Vertically, these meanderings and transport take place in the upper 1000m as narrow bands of 20-50 km (Figure 9). The southward flows of 10-40 cm/sec carry warm but relatively fresh ACC waters on the left and shelf waters on the right, as indicated by the high ^{228}Ra concentration. In general, shelf waters below the surface mixed layer become warmer and fresher moving to the northeast. The northward transport over the upper 1000m at the second and third separation bands are approximately 9 Sv (1 Sv=10^6 m^3/sec) and 18 Sv, respectively.

Model distributions of ^{228}Ra along the PR-SSR transect (see Figure 1b) indicate that the shelf waters being transported downstream are mainly associated with two fronts: 1) the Weddell-shelf front at 61.7^{o}S between the crossover portion of Weddell Slope waters and AP shelf waters, and 2) the shelf-ACC front at 60.7^{o}S (Figure 10). As noted above, the high ^{228}Ra shelf waters occupy the southern branch (right side) of the shelf-ACC front. The Weddell-shelf front has a width of ~20km and a current speed of ~15 cm/sec positioned at 1000-2000 m over the southern slope of Philip Ridge, while the shelf-ACC front has a width of ~30km and a speed decreasing from 40 cm/sec at the surface to 10 cm/sec at 1000 m. On average, the annual volume transport of shelf

waters (excluding the ACC part) by these two fronts in the upper 1000 m is approximately 1.5 and 3.0 Sv, respectively.

3.4. Seasonal cycles of the hydrographic conditions and circulation in the AP shelf

It is well known that there is strong seasonal variability in the meteorological processes over the AP shelf region (Figure 11). In particular, strong cooling in austral winter is associated with strong surface winds, which are in sharp contrast with the mild warming with relatively weak winds in austral summer. Surface precipitation is generally less than 0.3 cm/day and strongest in austral summer and winter, and spatially dominated by the northern SSIs shelf/slope region. This is comparable to, but lower than, the precipitation further south in the WAP (see, e.g., van Lipzig et al. 2004).

Model results show significant seasonal variability of temperature (not shown) and salinity along the BS transect (Figure 12, left panel). In association with winter cooling and summer warming, the surface temperature is lowest in winter at about -2^{o}C across the BS and the SSIs shelf, and highest in summer at around 0-2 ^{o}C with a strong N-S gradient. Similar to the model results, von Gildenfeldt et al. (2002) reported water temperatures of about -1.5^{o}C in winter and -0.7^{o}C in summer at the tip of AP. In association with surface precipitation and sea ice melting, modeled salinity is lowest during fall and spring and highest in winter. Spatially, the salinity has a strong N-S gradient throughout the year as noted above. At the tip of the AP, modeled salinity is about 34.2 psu in summer and 34.5 psu in winter, which is somewhat lower but comparable to the 34.5-34.6 psu as observed by von Gildenfeldt et al. (2002).

In contrast, modeled currents over the AP shelf are generally stable in terms of both general spatial patterns and values (Figure 12, right panel). Consistent with long-term mooring observations by von Gildenfeldt et al. (2002), CC is strongest during austral winter and spring

months, whereas the currents associated ASF and WF are generally quite stable. Model results suggest that the SBACC is strongest during late austral spring and weakest in austral winter. Among the major currents, the SBSC is not only weakest but also may change in strength, position, and direction. The currents over the inner shelf of SSIs are also weak at around 10 cm/sec and generally southwestward, consistent with the drifter movements in this area (Ardelan et al., 2009; Thompson et al., 2009). Surface winds appear to have no correlation with the SBSC, CC or currents in the northern SSIs shelf. In contrast, the BSC is strongest during austral fall in response to surface winds. The correlation coefficient between E-W component over the SSIs shelf and BSC during 2004 is r=0.46 (p<0.01) (Table 1).

In the surface layer, the salinity within the off-shelf transport bands northeast of EI are usually high except during the austral spring and fall, when the AP shelf waters are most fresh due to surface precipitation or ice melting (Figure 13, left panel). Naturally, temperature is lowest in austral winter and highest in summer (not shown). The three bands of off-shelf transport, however, persist throughout the year, with occasional breakdowns (Figure 13, right panel). A significant seasonality exists in these transport processes, which are strongest during austral spring and fall and are significantly correlated with the SBACC. For example, the off-shelf transport at around 54^{o}W has a correlation coefficient r=0.52 (p<0.01) in 2004 (Table 1, Figure 14). In contrast, surface winds have no significant correlation with these off-shelf transport terms (Table 1, Figure 14).

4. Discussion

4.1. The circulation around Antarctic Peninsula shelf region

Model results suggest that topographic steering largely controls the circulation pattern over the AP shelf region, at least on a monthly time-scale. On a monthly average the currents are in near geostrophic balance with the Rossby number $Ro=\zeta/f$ <0.1, where ζ is the relative vorticity and f is the Coriolis parameter, over much of the AP shelf region including outer SSIs shelf, BS, and northwestern Weddell shelf except in EITMZ, where strong nonlinearity is found with Ro >0.5 (not shown). A weak nonlinearity with Ro~0.2 can also be seen over the deep channel between the eastern basin of Bransfield Strait and Powell Basin, where a portion of the ASC turns into the BS. It is worth noting that the model may have under-predicted nonlinearity within the BS because of the relatively coarse model grid resolution (2 km), and the monthly forcing used. However, modeled weak nonlinearity within the BS on a monthly time-scale is still qualitatively consistent with the near geostrophic balance of currents reported by previous studies (Niiler et al. 1991; Gomis et al. 2002; Zhou et al. 2002, 2006). A recent analysis of drifter data by Thompson et al. (2009) also found that currents in this area strongly follow the contours of potential vorticity f/h, where h is the water depth, with eddies providing the major dispersion of tracers crossing the contours.

The strength of the AP shelf circulation is likely controlled by large-scale boundary forcing, surface winds, and, to a lesser extent, freshwater input. The ASC is a barotropic and nearly geostrophic western boundary current that is largely controlled by Sverdrup transport within the Weddell Gyre with possibly bottom intensification and increasing transport toward the north due to descending winter waters from the shelf (Muench and Gordon, 1995; Heywood et al., 2004; Thompson and Heywood, 2008). While a majority of the ASC circulates around Powell Basin, a

small portion of the current would either turn into BS or crossover the Philip Ridge to interact with ACC-shelf waters in the EITMZ. Therefore, the strength of ASC will likely affect the BS circulation and/or complex transport and mixing around Elephant Island.

The CC, in contrast, is largely maintained by surface winds and the density gradient between cold shelf waters and relatively warm Weddell slope water with a speed of ~10 cm/sec and a water depth range of 100-500 m (Figure 9; von Gildenfeldt et al. 2002; Heywood et al., 2004). Since the CC converges with the ASC at the tip of the AP and then turns southwestward into the BS, this current will also affect the water properties and transport in the strait.

Model results suggest that transport rates of the CC and ASC at the Joinville Ridge segment are approximately 2 Sv and 18 Sv, respectively, which are close to the estimates by recent observation-based studies (Muench and Gordon, 1995; Heywood et al., 2004), and a numerical model (Matano et al., 2002). This is lower, however, than the recent estimate of 48 Sv by Thompson and Heywood (2008), which includes the volume transport of deep water flow that is likely underestimated in our model. Model results further suggest that, among these transports, about 2 Sv turns into the BS, which falls between the 1 Sv estimate of Heywood et al. (2004) and the 2.4±1 Sv estimate of von Gyldenfeldt et al. (2002).

The impacts of SBACC on the circulation over the AP shelf region remain unclear. Model results show that the ACC-shelf mixed waters in the WAP may cross over the shallow sills between Brabant Island and Smith Island, and intrude into the BS (Figure 8). But the volume of the intrusion through this route appears to be limited (Capella et al. 1992; Gomis et al., 2002; Zhou et al., 2002). Capella et al. (1992) suggested that the ACC waters enter the strait mainly through the deep trough between Smith Island and Livingston Island. Zhou et al. (2006) were able to identify waters with similar characteristics (warm and salty) as those of the UCDW at

300-500 m over the KGI slope area (BS side), which are similar to the warm and salty waters observed during the NBP0606 cruise (Figure 4a, c). However, no significant intrusion of the UCDW is present the model results (Figure 4b, d).

Over the SSIs northern shelf margin, the Ekman transport driven by prevailing westerly winds likely transport the shelf waters towards the offshore area, and induce subsurface upwelling of UCDW onto the shelf at the same time. In addition, the SBACC may penetrate into the BS through the channel between KGI and EI (Figure 8, Thompson et al., 2009).

The model appears to have underestimated the strength of BSC for several reasons. Firstly, the transport by Gerlache Strait Current is likely underestimated due to the much shallower water depth in the model. Secondly, the intruding flow of upper CDW into the BS is largely missing, which is likely due to the smoothing of bottom topography, the coarse resolution of the model, and the weaker than expected non-geostrophic currents due to the smooth monthly winds. Thirdly, the broader width of the BSC may be simply due to the coarse model resolution (~2 km).

4.2. Off-shelf transport around the Elephant Island

The circulation in the EITMZ is highly dynamic driven by the complicated interactions between the ACC, BSC, and Weddell Sea currents over a complex bathymetry. Both model results and observations indicate that as the SBACC and a portion of SACCF pass through the SFG where the currents become stronger (> 50 cm/sec; Figures 2-3 and 8; Zhou et al. 2010). A portion of the combined flow turns northward along the eastern side of STR, likely constrained by the geostrophic balance (Zhou et al., this volume), a second part moves through the middle of the Ona Basin, and the remaining flow detours southeastward following the shelf slope. The third part of the flow largely follows the contours of potential vorticity *f/h* through the topographic

features including Shackelton Bank and Terror Rise (Figures 2, 8 and 9). Nevertheless, the relatively strong nonlinearity of these currents allows them to cross the *f/h* contours and hence drive strong horizontal mixing and diffusion. A portion of the Weddell Slope Current is able to cross the Hesperides Trough to join the northeastward currents over the northern slope of the South Scotia Ridge (Figures 2, 8, and 10), consistent with drifter trajectories (Thompson et al. 2009).

The currents over the AP shelf region (SSIs shelf-break current, BSC, ASC) all converge and transport cold and salty shelf waters toward EI, where intense off-shelf transport and mixing between the ACC and shelf waters take place (Figures 2 and 8; Zhou et al., this volume). The total transport of these currents is about 4.5 Sv (see section 3.3; Figure 10). Therefore, shelf circulation contributes about 50% of the total off-shelf transport at the second separation band northeast of EI (Figure 9). Strong horizontal mixing occurs between the ACC and shelf waters as they move downstream, as indicated by the third separation band in Figure 9. In addition, within the upper 500 m, shelf waters are generally denser than the ACC waters. Therefore the shelf waters tend to sink deeper along the isopycnals as they move offshore (Frants et al. this volume), which also reduces the horizontal density gradient.

The strong nonlinearity of the currents in the EITMZ ensures strong horizontal turbulent mixing. Dulaiova et al. (2008) estimated that the horizontal scale of short-lived ^{224}Ra along the EI-SFG segment in January 14-February 8 was about 150km, which is equivalent to a horizontal diffusivity of 6×10^4 m^2/sec. Using the same method as Dulaiova et al. (2009) and a simulation of ^{224}Ra (not shown), our modeled effective eddy diffusivity in this region during summertime can be estimated to be about 10^3 m^2/sec with a corresponding horizontal scale about 40 km. Therefore, the model may have under-estimated the horizontal diffusivity and hence the spatial

spreading of shelf waters in this area during summertime. This is consistent with the relatively weak mixing between the BS and ACC surface waters in summer 2004 as indicated by the salinity field in Figure 5c. The weaker horizontal mixing in the model could be due to a combination of weaker forcing (monthly winds), smoother topography and a weaker modeled BSC.

4.3. The sources of shelf waters in the EITMZ

In order to illustrate the sources of sediment input from the AP shelf region, we present a series of modeled surface distributions of an inert tracer during the first year since the beginning of the release (Figure 15). The tracer first reaches the surface at the shallow coastal areas around the SSIs and AP shelf region (Figures 15a). Those around the northern SSIs shelf are transported downstream by the shelfbreak current and some of them were entrained into the ACC waters as indicated by the tracer band over the northern SSIs slope area at around 61.6^{o}S (Figure 16a, b). The mixed waters continue northeast, reaching the Ona Basin in three months, and spreading into the southern Scotia Sea through the northern flank of the South Orkney Plateau in six months (Figure 15b). After six months, the tracer input from the western BS shelf areas and NW Weddell shelf is able to join the downstream waters in the EITMZ, mainly through the shelfbreak current with additional transport through the gap between EI and CI by the BSC. The strongest input to the surface waters, however, occurs in winter when relatively shallow water columns on shelf areas such as northwestern Weddell, the southern BS and northern SSIs shelves are well mixed (Figure 16c). After 9 months, some of the mixed waters turn southward being entrained into the Weddell Front along the western edge of the South Orkney Plateau (Figure 15c, d).

These model results and ^{228}Ra measurements during the AMLR 2006 cruise suggest that the mixed shelf-ACC waters northeast of Elephant Island can be derived from several sources. The major sources appear to be the shallow sills between Gerlache Strait and Smith Island at the western end of Bransfield Strait and the northern SSIs shelf region, where winter mixing allows surface waters to interact with the seafloor sediments (Figures 7, 15 and 16). The shelf area north of Livingston Island also exhibits relatively elevated ^{228}Ra concentration, ~7-8 (dmp/m^3), indicating a potential source (Figure 7d). Companion measurements of short-lived ^{224}Ra (a good indicator for local effects) during the same cruise more clearly indicate strong sediment sources in this area (Dulaiova et al. 2009). The BSC could also transport some of the sediment input in the BS through the gap between EI and CI. However, the model may have underestimated this contribution due to the underpredicted BSC and winter vertical mixing. Measurements of ^{228}Ra also suggest that sediment input around Joinville Island may be mixed to the surface during winter and then spread over toward the EI region by the crossover flow of the Weddell Front (Figure 7d). Model winter mixed layer in this area is too shallow and hence sediment input in this area is not present at the surface. Using the hydrographic data from the summer 2004 and winter 2006 cruises as well AMLR 2004 (summer) cruises, Frants et al. (this volume) found that the shelf waters from BS dominated the high Fe mixed waters in the northeast of EI, whereas the shelf waters from the northern SSIs shelf/slope also contributed to higher Fe mixed waters. Based on the characteristics of trace metals measured during the LMG0402 cruise, Measures et al. (this volume) argue that high Fe found northeast of EI is mainly from the shelf area surrounding SSIs and the western end of the BS, and they are unlikely to originate from upwelling of deep waters over the northern SSIs shelf/slope. Our Model results suggest that an additional contribution of the mixed shelf-ACC waters comes from the crossover flow of

1 Weddell Slope Current, consistent with the drifter analysis by Thompson et al. (2009) (Figures 2
2 and 8). However, the majority of this input is likely Fe-poor as suggested by the Fe
3 measurements along a transect extending from EI into the Powell Basin during the NBP0606
4 cruise (Hatta et al., this volume).
5

5. Conclusions

A numerical model based on ROMS has been developed for the Antarctic Peninsula, Drake Passage, Scotia Sea, and northern Weddell Sea region. The model has been spun-up for three years with climatological forcing and a realistic simulation for 2004-2006 has been carried out with monthly forcing from observed data, NCEP re-analysis output and a global circulation model (OCCAM) output. The model results are analyzed to understand the seasonal variability of circulation in the AP shelf region and the off-shelf transport in the northeast of Elephant Island. A naturally occurring tracer (radium isotope ^{228}Ra) is also included in the model to investigate the sediment nutrient (including Fe) input to the shelf region, and the subsequent transport and dispersion to southern Drake Passage and Scotia Sea.

The model results suggest a persistent and coherent circulation pattern over much of the AP shelf region throughout the year consisting of several major components that converge water masses from various sources toward Elephant Island. These currents are largely in geostrophic balance, mainly driven by surface winds, topographic steering and large-scale forcing. Strong off-shelf transport of the Fe-rich shelf waters takes place over the northeastern shelf/slope of Elephant Island (EITMZ), driven by a combination of topographic steering, extension of shelf currents, and strong horizontal mixing between ACC and shelf waters. Both the shelf circulation and off-shelf transport show a significant seasonality, likely driven by strong seasonal variations of surface winds and large scale forcing. These results are generally consistent with historical studies and our recent field surveys. The model, however, likely under-estimates the vertical mixing overall and the seasonality of currents in the AP shelf region due to the monthly forcing applied.

Modeled and observed distributions of ^{228}Ra suggest that a majority of Fe-rich surface waters exported off-shelf around Elephant Island are from the shallow sills between Gerlache Strait and Livingston Island, and northern shelf of the South Shetland Islands carried by the shelfbreak current and the Bransfield Strait Current. The shelf region at the tip of the Antarctic Peninsula including eastern BS shelf and northwestern Weddell Shelf likely also contributes to the surface waters downstream. The vertical Fe flux is largely due to strong winter vertical mixing, which brings surface water in contact with the shelf sediment in the relatively shallow areas. This vertical Fe flux, however, is likely under-estimated by the model because of the weak vertical mixing driven by the monthly forcing.

Acknowledgements: This project is supported by NOAA grant NA09OAR4310062. MZ and MJ are also supported by NSF grant 0948378 and MAC by NSF grant 0948442. The satellite altimetry data is provided by AVISO (http://www.aviso.oceanobs.com/). We thank the OCCAM modeling group for providing their long-term global model output (http://www.noc.soton.ac.uk/JRD/OCCAM/EMODS/info/coord.php3). Relative humidity and precipitation data are provided by HOAPS project from http://www.hoaps.zmaw.de/index.php?id=home. We thank Kate Hedstrom at the University of Alaska at Fairbank for providing the ROMS model with imbedded sea ice component. The numerical computation is carried out at the cluster computer RAVANA at the University of Massachusetts Boston.

References

Amos, A.F., 2001, A decade of oceanographic variability in summertime near Elephant Island, Antarctica, J. of Geophys. Res. 106, 22,401-22,423.

Andersson, A., K. Fennig, C. Klepp, S. Bakan, H. Gral, and J. Schulz, 2010, The Hamburg Ocean Atmosphere Parameters and Fluxes from Satellite Data - HOAPS-3, *Earth Syst. Sci. Data Discuss.*, **3**, 143-194, doi:10.5194/essdd-3-143-2010.

Antonov, J. I., D. Seidov, T. P. Boyer, R. A. Locarnini, A. V. Mishonov, H. E. Garcia, O. K. Baranova, M. M. Zweng, and D. R. Johnson, 2010. *World Ocean Atlas 2009, Volume 2: Salinity.* S. Levitus, Ed. NOAA Atlas NESDIS 69, U.S. Government Printing Office, Washington, D.C., 184 pp.

Ardelan, M. V., O. Holm-Hansen, C. D. Hewes, C. S. Reiss, N. S. Silva, H. Dulaiova, E. Steinnes, and E. Sakshaug, 2009, Natural iron enrichment around the Antarctic Peninsula in the Southern Ocean, Biogeosciences Discuss., 6, 7481–7515

Brandon, M.A., M. Naganobu, D. A. Demer, P. Chernyshkov, P. N. Trathan, S. E. Thorpe, T. Kameda, O. A. Berezhinskiy, E. J. Hawker, and S. Grant, 2004, Physical oceanography in the Scotia Sea during the CCAMLR 2000 survey, austral summer 2000, Deep-Sea Research II 51: 1301–1321.

Capella, J., R. Ross, L.B. Quetin, and E.E. Hofmann, 1992, A note on the thermal structure of the upper ocean in the Bransfield Strait-South Shetland Islands region. Deep-Sea Research I, 39 (7–8), 1221–1229.

Charette, M. et al. 2007, Radium isotopes as tracers of iron sources fueling a Southern Ocean phytoplankton bloom, Deep-Sea Res. II, 54, 18-20.

Collins, W. D., C. M. Bitz, M. L Blackmon, G. B. Bonan, C. S. Bretherton, J. A Carton, et al.

2006, The Community Climate System Model Version 3 (CCSM3), *Journal of Climate*, 19(11), 2122-2143.

Cunningham, S. A., S. G. Alderson, and B. A. King, M. A. Brandon, 2003, Transport and variability of the Antarctic Circumpolar Current in Drake Passage, J. Geophys. Res., 108(C5), 8084, doi:10.1029/2001JC001147.

Da Silva, A., A. C. Young, and S. Levitus, 1994, Atlas of surface marine data 1994, volume 1: Algorithms and procedures, Tech. Rep. 6, U.S. Department of Commerce, NOAA, NESDIS.

Ducklow, H. W., K. Baker, W.R. Fraser, D.G. Martinson, L.B. Quetin, R.M. Ross, R.C. Smith, S. Stammerjohn, and M. Vernet, 2007, Marine ecosystems: theWest Antarctic Peninsula. Phil. Trans. R. Soc. B 362, 67–94.

Dulaiova, H. et al. 2009, Shelf-derived iron inputs drive biological productivity in the southern Drake Passage. Global Biogeochemical Cycle. GB4014. Vol. 23.

Frants, M., S T. Gille, C. D. Hewes, O. Holm-Hansen, M. Kahru, A. Lombrozo, C. I. Measures, B. G. Mitchell, H. Wang, and M. Zhou, this volume, Optimal Multi-parameter Analysis of source water distributions in the Southern Drake Passage.

Gomis D., M. A. Garcia, O. Lopez, and A. Pascual, 2002, Quasi-geostrophic 3D circulation and mass transport in the western Bransfield Strait during Austral summer 1995/96. Deep-Sea Research II 49: 603–621.

Hatta, M. et al. this volume, Iron fluxes from the shelf regions near the South Shetland Islands in the Drake Passage during the austral-winter 2006.

Heywood, K.J., A.C.N. Garabato, D. P. Stevens, and R. Muench, 2004, On the fate of the Antarctic Slope Front and the origin of the Weddell Front, J. Geophys. Res. 109, C06021.

Holm-Hansen**, O.**, M. Kahru, C.D. Hewes, S. Kawaguch, T. Kameda, V.A. Sushin, I. Krasovski, J. Priddle, R. Korb, R.P. Hewitt, and B.G. Mitchell, 2004, Temporal and spatial distribution of chlorophyll-a in surface waters of the Scotia Sea as determined by both shipboard measurements and satellite data, Deep-Sea Research II, 51:1323–1331

Hunke, E. C., 2001: Viscous-plastic sea ice dynamics with the EVP model: linearization issues, *J. Comp. Phys.*, **170**, 18-38.

Hunke, E. C. and J. K. Dukowicz, 1997: An elastic-viscous-plastic model for sea ice dynamics, *J. Phys. Oceanogr.*, **27**, 1849-1868.

Kahru, M., et al., 2007, Eddies enhance biological production in the Weddell-Scotia confluence of the Southern Ocean. Geophys. Res. Lett., 34 (14): L14603. DOI: 10.1029/2007GL030430.

Kalnay, E., M. Kanamitsu, R. Kistler, W. Collins, D. Deaven, and co-authors. 1996, The NCEP/NCAR re-analysis project. Bull. Amer. Meteor. Soc. 77, 437–471.

Korb, R.E., M. J. Whitehouse, M. Gordon, P. Ward, and A. J. Poulton, 2010, Summer microplankton community structure across the Scotia Sea: implications for biological carbon export, Biogeosciences, 7, 343–356.

Large, W.G., McWilliams, J.C., Doney, S.C., 1994. Oceanic vertical mixing: a review and a model with a nonlocal boundary layer parameterization. Reviews of Geophysics 32 (4), 363–403.

Locarnini, R. A., A. V. Mishonov, J. I. Antonov, T. P. Boyer, H. E. Garcia, O. K. Baranova, M. M. Zweng, and D. R. Johnson, 2010. *World Ocean Atlas 2009, Volume 1: Temperature.* S. Levitus, Ed. NOAA Atlas NESDIS 68, U.S. Government Printing Office, Washington, D.C., 184 pp.

Matano, R. P., A. L. Gordon, R. D. Muench, and E. D. Palma, 2002, A numerical study of the circulation in the northwestern Weddell Sea, Deep Sea Res., Part II, 49, 4827– 4841.

Martin, J.H., R.M. Gordon, and S.E. Fitzwater, 1990, Iron in Antarctic waters. Nature 345: 156-158.

Measures, C.I. et al. this volume, The influence of shelf processes in delivering dissolved iron to the HNLC waters of the Drake Passage, Antarctica.

Mellor, G. L. and L. Kantha, 1989, An ice-ocean coupled model, *J. Geophys. Res.*, **94**, 10,937-10,954.

Muench, R.D., and A.L. Gordon, 1995, Circulation and transport of water along the western Weddell Sea margin, J. Geophys. Res., 100(C9), 18,503-515.

Nelson, DM and W.O. Smith, 1991, Sverdrup revisited – critical depths, maximum chlorophyll levels, and the control of Southern Ocean productivity by the irradiance-mixing regime, Limnol. and Oceanogr., 36(8): 1650-1661.

Niiler, P.P., A.F. Amos, and J.-H. Hu, 1991, Water masses and 200m relative geostrophic circulation in the western Bransfield Strait region. Deep-Sea Research II 38, 943–959.

Orsi, A. H., T. Whitworth, and W.D. Nowlin, 1995, On the meridional extent and fronts of the Antarctic circumpolar current. Deep-Sea Res. I. 42: 641-673.

Shchepetkin, A.F., and J.C. McWilliams, 2003, A method for computing horizontal pressure-gradient force in an oceanic model with a non-aligned vertical coordinate. J. Geophys. Res. 108 (C3), 3090.

Shchepetkin, A.F. and J. C. McWilliams, 2005, The regional oceanic modeling system (ROMS): a split-explicit, free-surface, topography-following-coordinate oceanic model. Ocean Modelling, 9: 347–404.

Smagorinsky, J., 1963, General circulation experiments with the primitive equations, Mon. Weather Rev., 91: 99–164.

Smolarkiewicz, P. K., 1984, A fully multidimensional positive-definite advection transport algorithm with small implicit diffusion. *J. Com- put. Phys.*, 54, 325–362.

Thompson, A.F., and K. J. Heywood, 2008, Frontal structure and transport in the northwestern Weddell Sea, Deep-Sea Research I 55, 1229– 1251.

Thompson, A.F., K. J. Heywood, S.E. Thorpe, A.H.H. Renner, and A. Trasvina, 2009, Surface Circulation at the Tip of the Antarctic Peninsula from Drifters, J. Phys. Oceanogr., 39, 3-26.

Thorpe, S.E. et al. 2005, Comparison of two time-variant forced eddy-permitting global ocean circulation models with hydrography of the Scotia Sea. Ocean Modelling 9: 105–132.

van Lipzig, N.P.M., J.C. King, T.A. Lachlan-Cope, and M.R. van den Broeke, 2004, Precipitation, sublimation, and snow drift in the Antarctic Peninsula region from a regional atmospheric model. Journal of Geophysical Research 109, D24109.

von Gyldenfeldt, A. B., E. Fahrbach, M. A. Garcıa, and M. Schroder, 2002, Flow variability at the tip of the Antarctic Peninsula, Deep Sea Res., Part II, 49, 4743– 4766.

Vaughan, D. G., G.J. Marshall, W.M. Connolley, C. Parkinson, R. Mulvaney, D. Hodgson, J.C., King, C. J. Pudsey, and J. Turner, 2003, Recent rapid regional climate warming on the Antarctic Peninsula. Clim. Change 60, 243–274.

Webb, D.J., B. A. de Cuevas and A. C. Coward, 1998, The first main run of the OCCAM global ocean model, Southampton Oceanography Centre, Internal Document No. 34.

Zhou, M., Niiler, P.P., Hu, J.-H., 2002. Surface current in the Bransfield and Gerlache Straits measured by surface Lagrangian drifters. Deep-Sea Research I 46, 267–280.

Zhou, M., Pearn, P., Zhu, Y., Dorland, R., 2006, The western boundary current in the Bransfield Strait, Antarctica, Deep-Sea Res. I, 53: 1244-1252.

Zhou, M., Y. Zhu, and R.D. Dorland, 2010, Dynamics of the current system in the southern Drake Passage. Deep-Sea Res. I, 57, 1039-1048.

Zhou, M. et al., this volume, Winter mesoscale circulation on the shelf slope region of the southern Drake Passage.

Table 1. Correlation matrix between modeled major currents and surface wind stress in 2004*.

Correlation (r)	τ_x	SBACC	BSC	CC	V_{EI}
τ_x	1				
SBACC	**-0.25**	1			
BSC	**0.46**	**-0.57**	1		
CC	0.64	**-0.47**	**0.47**	1	
V_{EI}	0.07	**0.53**	-0.19	-0.15	1

*Bold values indicate significant correlation.

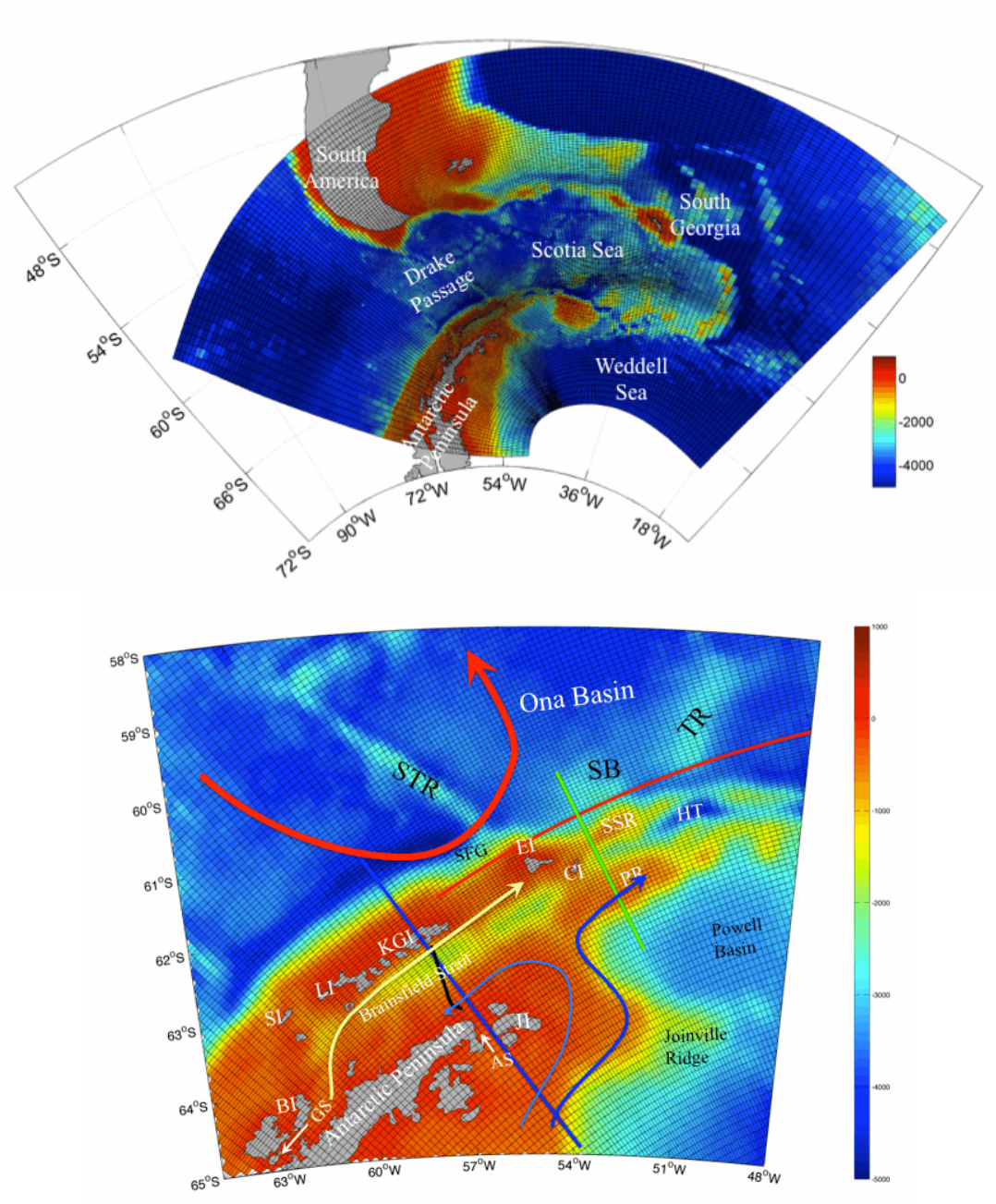

Figure 1. Top panel: Model domain (one per every three grid lines is plotted) and bathymetry. Bottom panel: model grid for the Antarctic Peninsula area (one per two grid lines is plotted). Red, blue and green lines indicate the model Elephant Island slope transect, BS transect, and PR-SSR transect, respectively. Black line indicates the observed BS transect during NBP0606 cruise. Acronyms: BI – Brabant Island, GS – Gerlache Strait, AS – Antarctic Sound, JI – Joinville Island, SI – Smith Island, LI – Livingston Island, KGI –King George Island, EI – Elephant Island, CI – Clarence Island, SSR – South Scotia Ridge, PR – Philips Ridge, HT – Hesperides Trough, STR – Shackelton Transverse Ridge, SFG – Shackelton Fracture Gap, SB – Shackelton Bank, TR – Terror Rise. South Shetland Islands (SSIs) referred to the island chains including SI, LI, and KGI. Broad arrows indicate the dominant currents (for details see text).

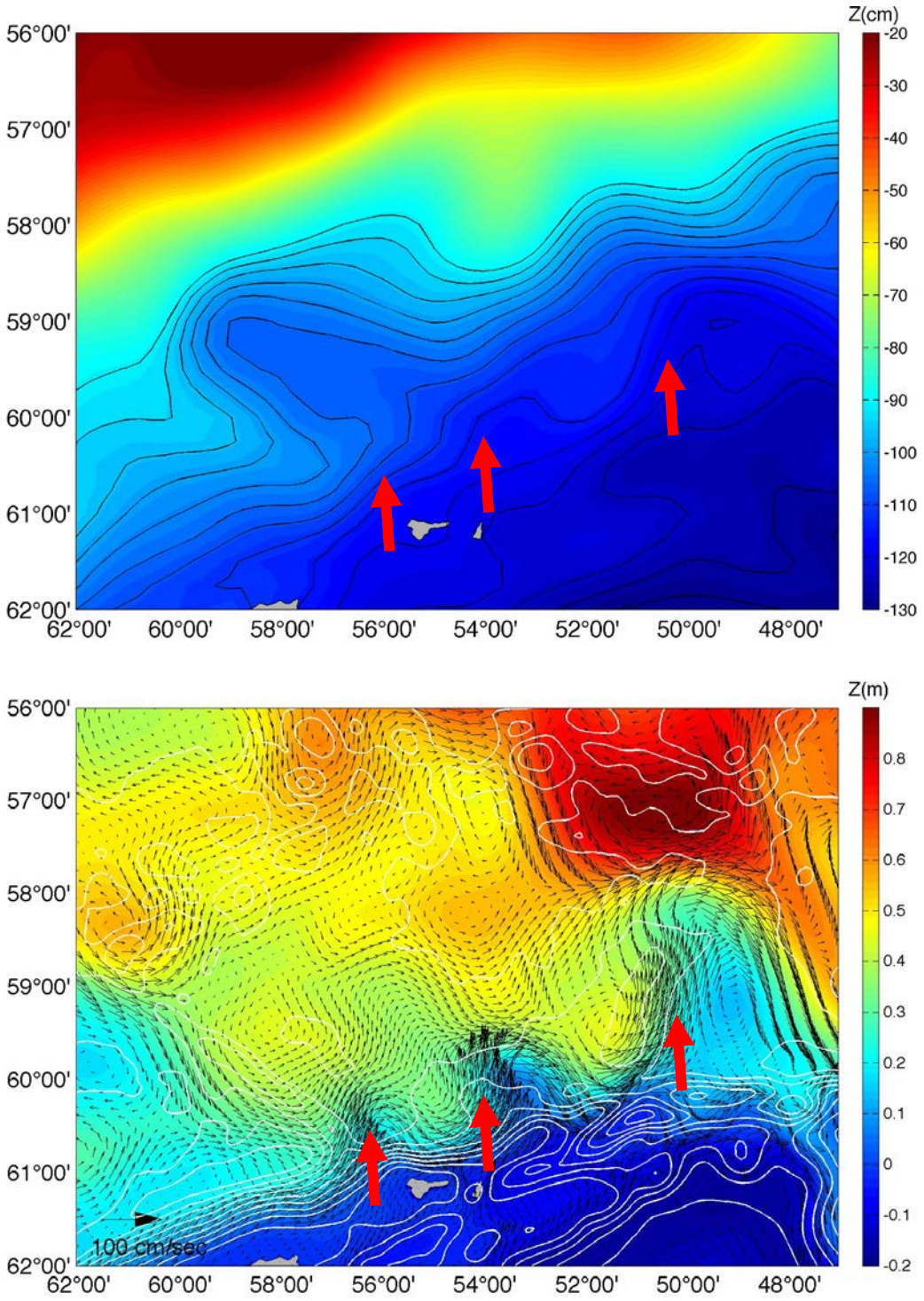

Figure 2. Top panel: Long-term (1986-2010) mean sea surface dynamic height (cm) from AVISO. Bottom panel: Model annual mean surface currents (arrows) and sea level (m, color) in 2004. Red broad arrows highlight the off-shelf transport points.

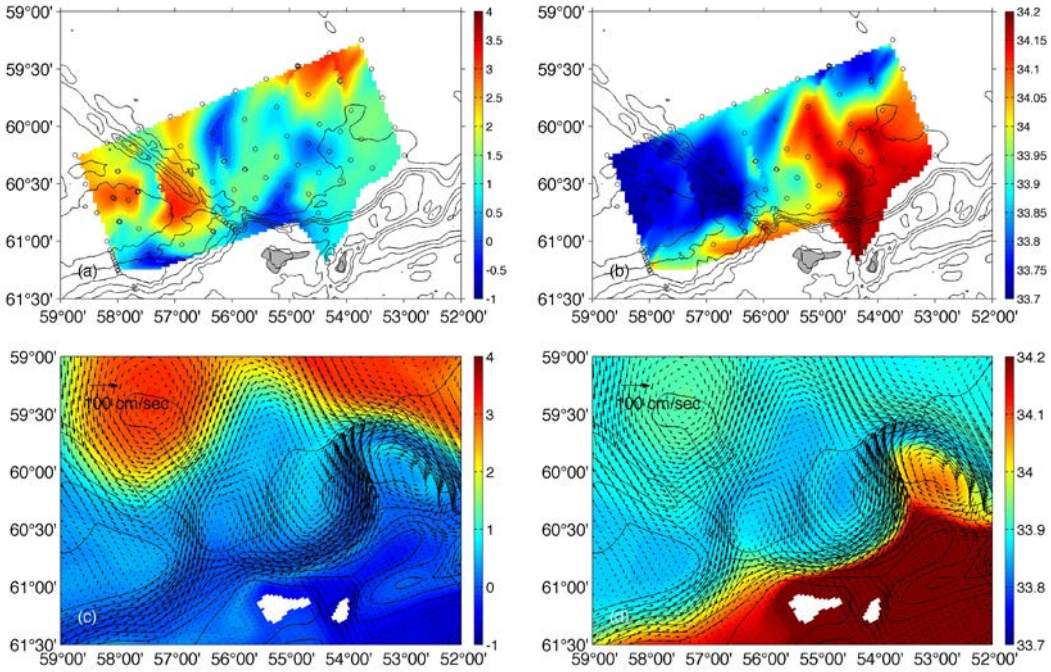

Figure 3. Observed temperature (^{o}C, top left) and salinity (psu, top right) at 50m in Feb. 25-Mar. 24, 2004, and model temperature (^{o}C, bottom left) and salinity (psu, bottom right) and currents at 50m in February 2004 (monthly averages).

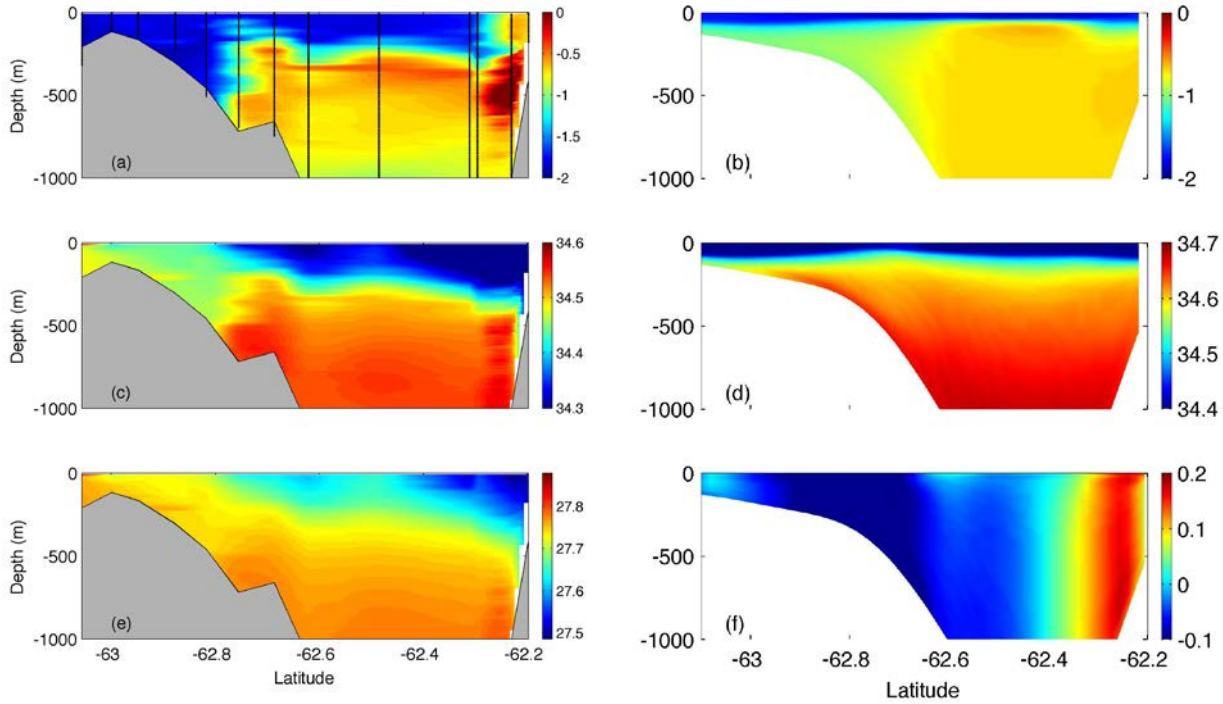

Figure 4. Left panels: (a) Observed temperature (^{o}C), (c) salinity (psu) and (e) density (kg/m^{3}) along the BS transect (see Figure 1b) in the middle of Bransfield Strait (July 25-August 15, 2006). Right panels: (b) modeled temperature (^{o}C), (d) salinity (psu) and (f) along-shelf current (m/sec, eastward positive) in August 2006 (monthly averages). Note the different color-scale between panels.

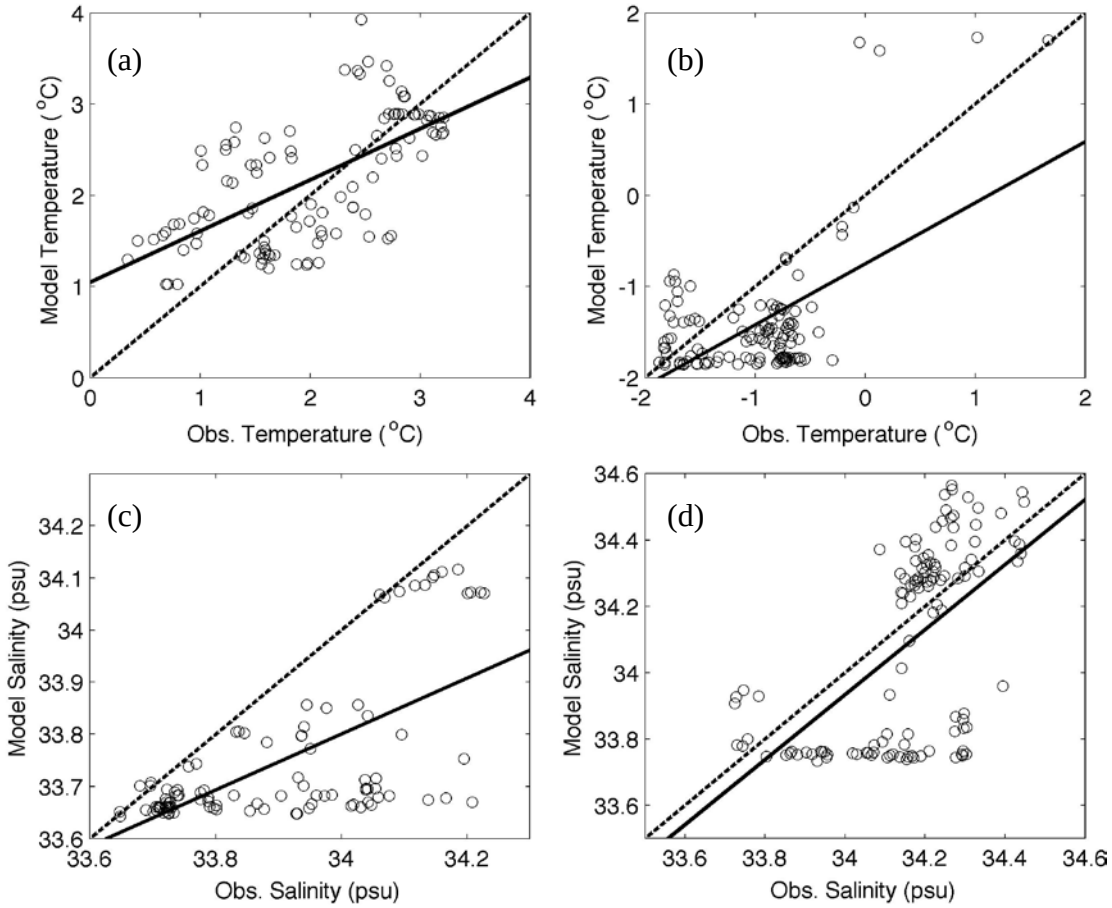

Figure 5. One-to-one correlations between modeled and observed 10 m temperature and salinity in summer 2004 and winter 2006: (a) model 10m temperature in February 2004 (monthly average) versus observed temperature during February-March 2004 (r=0.66, p<0.01), (b) model 10m temperature in August 2006 (monthly average) versus observed temperature during July-August 2006 (r=0.58, p<0.01), (c) same as (a) except for salinity (r=0.61, p<0.01), and (d) same as (b) except for salinity (r=0.56, p<0.01). Solid lines are least-square regressions and dashed lines indicate the 1:1 relationship. The locations of LMG0402 stations please see Figure 3a. The locations of NBP0606 stations see Zhou et al. (this volume).

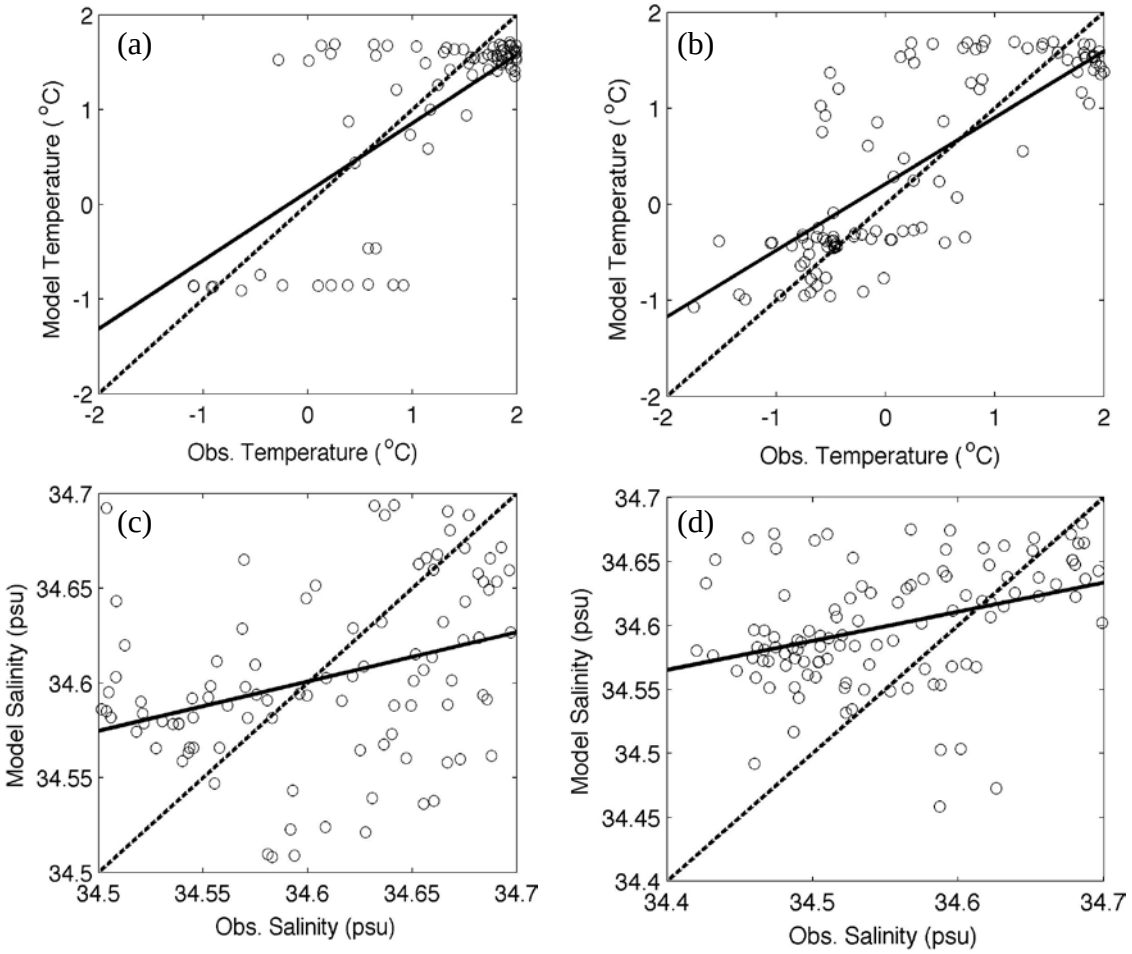

Figure 6. Same as Figure 5 but for 400 m: (a) model temperature in February 2004 (monthly average) versus observed temperature during February-March 2004 (r=0.75, p<0.01), (b) model temperature in August 2006 (monthly average) versus observed temperature during July-August 2006 (r=0.84, p<0.01), (c) same as (a) except for salinity (r=0.34, p<0.01), and (d) same as (b) except for salinity (r=0.36, p<0.01). Solid lines are least-square regressions and dashed lines indicate the 1:1 relationship.

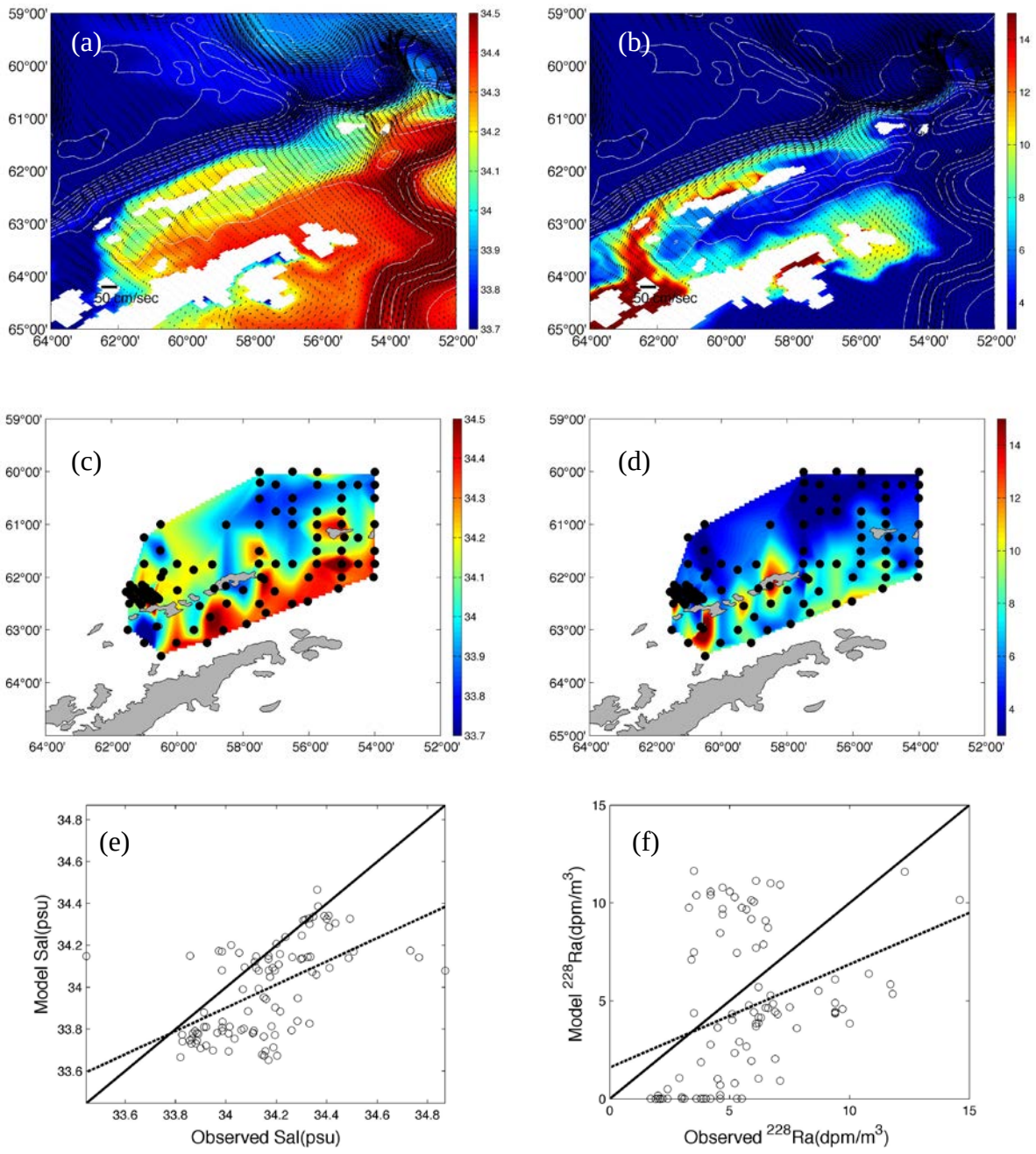

Figure 7. (a) Modeled surface salinity (psu) and (b) ^{228}Ra (dpm/m^3) in January 2006 (monthly averages), and (c) observed surface salinity (psu) and (d) ^{228}Ra (dpm/m^3) during January-February 2006. Also shown are 1:1 correlations between the modeled and observed salinity (r=0.56, p<0.01) (e) and ^{228}Ra (r=0.35, p<0.01) (f). In Figure 7d, a background value of 1.7 dpm/m^3 is subtracted from the observed ^{228}Ra concentration. Model values of ^{228}Ra are scaled to the observed ones since model sediment ^{228}Ra flux has an arbitrary unit.

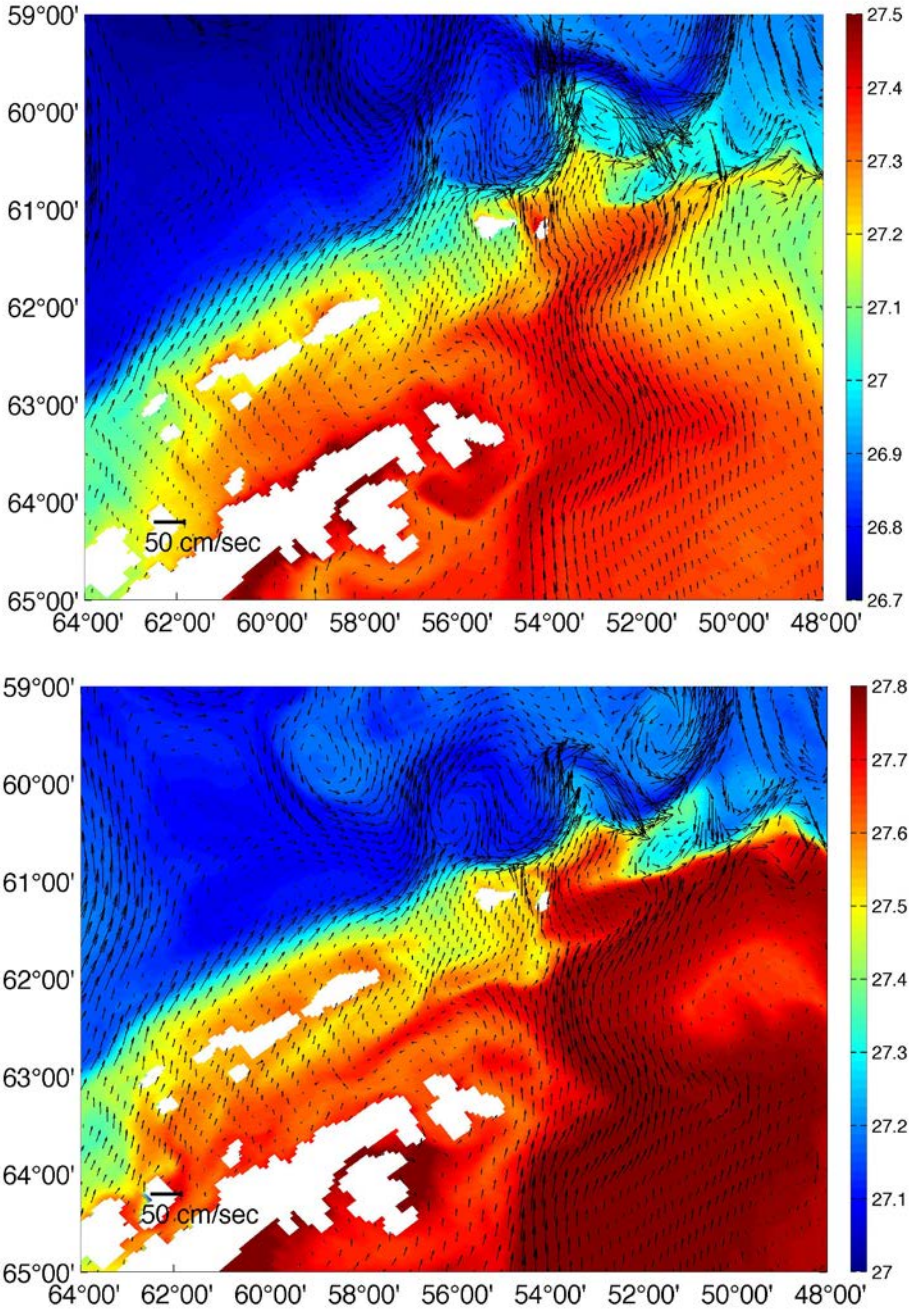

Figure 8. Monthly averaged model surface currents (m/sec, arrows) and density (kg/m^3, color) in February (top panel) and August 2004 (bottom panel).

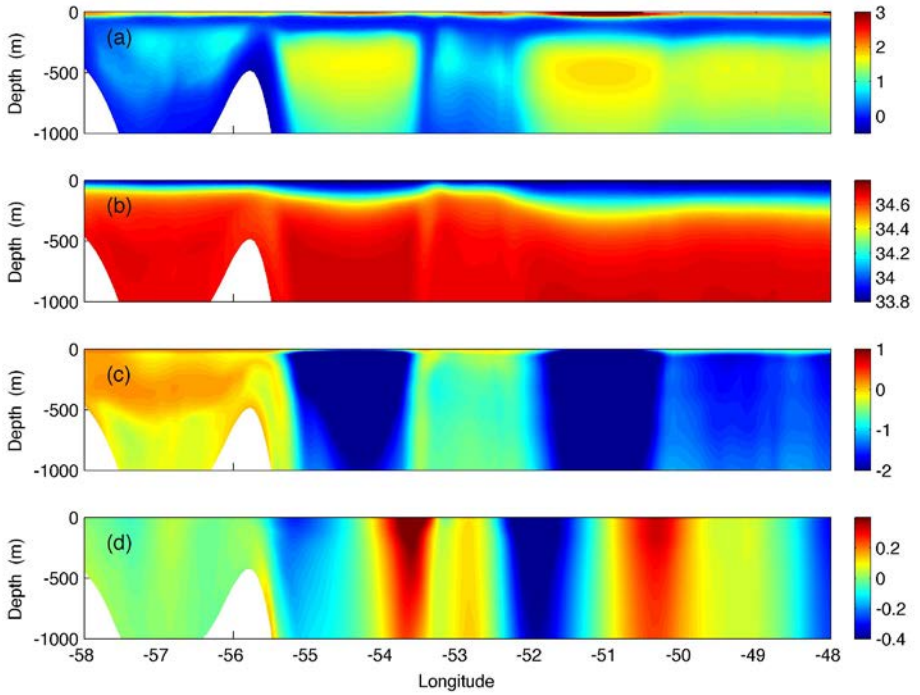

Figure 9. Monthly averaged model output along the section over the northern slope in March 2004 (see Figure 1): (a) Modeled temperature (^{o}C), (b) salinity (psu), (c) $\log_{10}(^{228}\text{Ra})$ (dpm/m^3), and (d) N-S velocity (m/sec, northward positive). The white caps mark the northern edge of the EI.

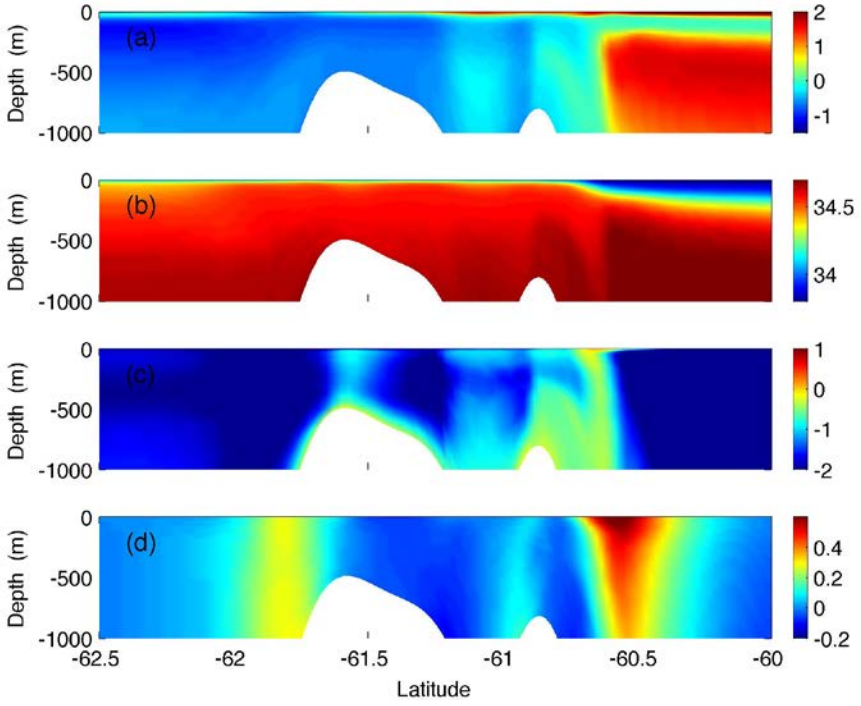

Figure 10. Monthly averaged model output along PR-SSR transect in March 2004: (a) temperature (^{o}C), (b) salinity (psu), (c) $\log_{10}(^{228}\text{Ra})$ (dpm/m^3), and (d) cross-transect velocity (m/sec, eastward positive).

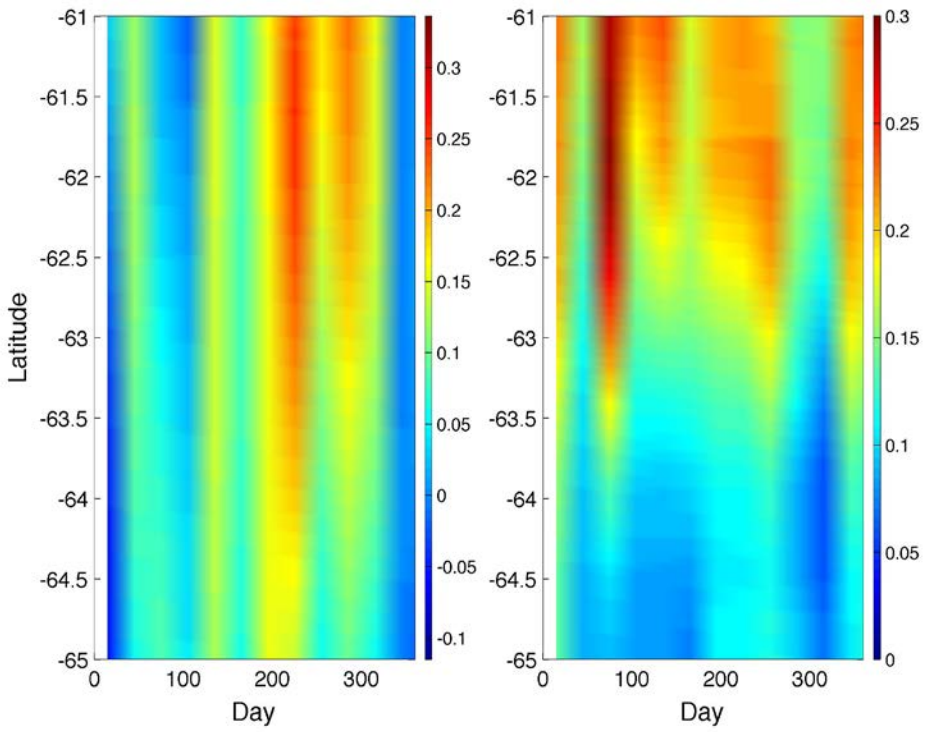

Figure 11. (left) Along-shelf wind stress (N/m^2) (northeastward positive), and (right) surface precipitation rate (cm/day) along the BS transect (see Figure 1b) in 2004.

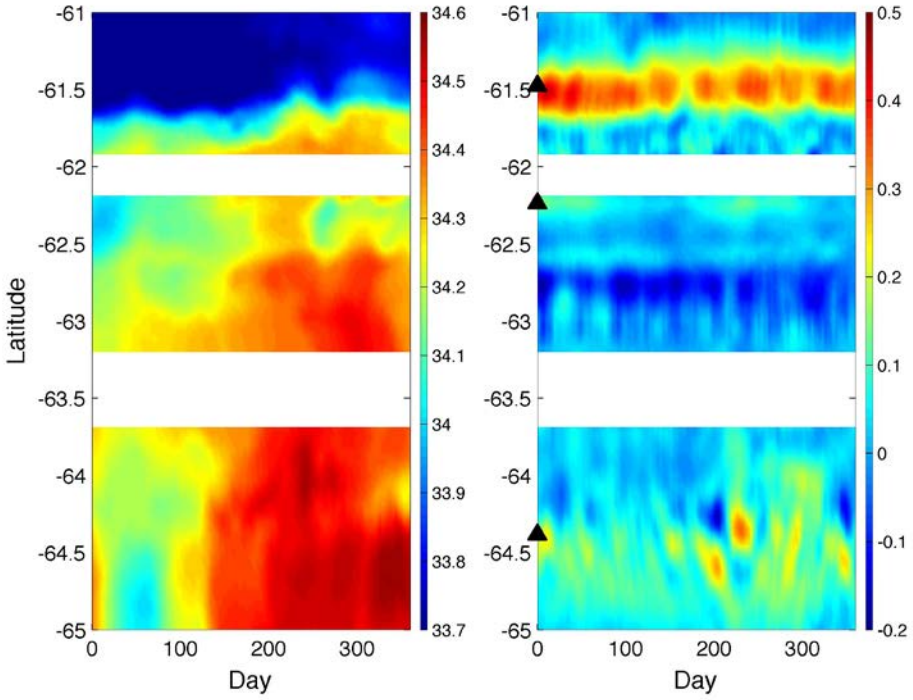

Figure 12. Seasonal cycle of surface (left) salinity (psu) and (right) along-shelf velocity (m/sec, eastward positive) along the BS transect (see Figure 1b) in 2004. Model results consist of snapshots with a 3-day interval. Three triangles in the right panel indicate the locations of the representative current velocities for SBACC, BSC and CC, respectively.

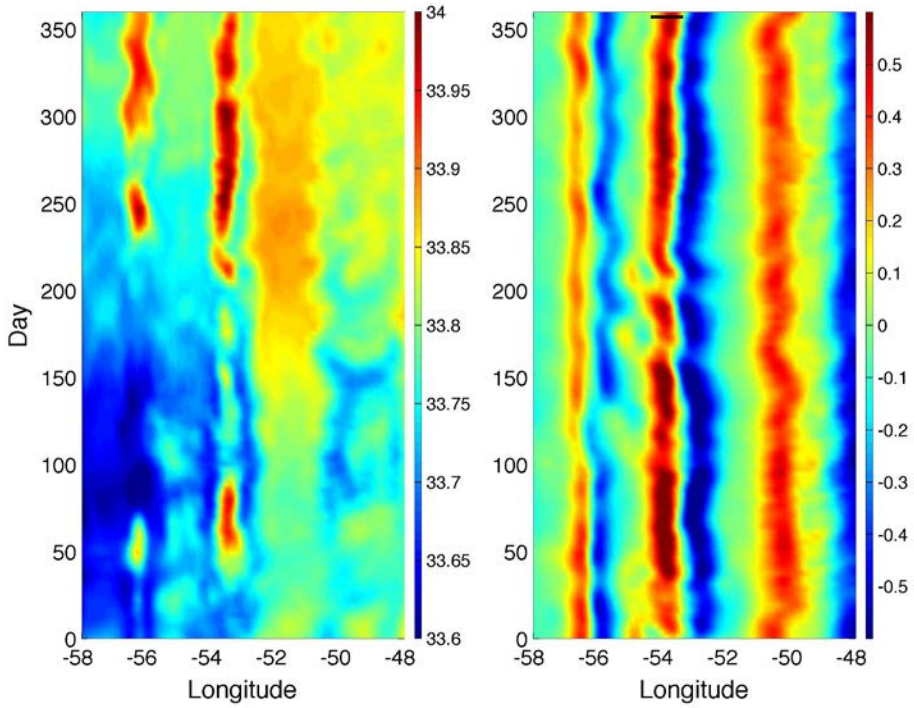

Figure 13. Seasonal cycle of surface (left panel) salinity (psu) and (right panel) cross-shelf velocity (m/sec, off-shelf positive) along the EI shelf slope transect (see Figure 1b) in 2004. Model results consist of snapshots with a 3-day interval. Black line on top of the right panel indicates average range for off-shelf transport velocity.

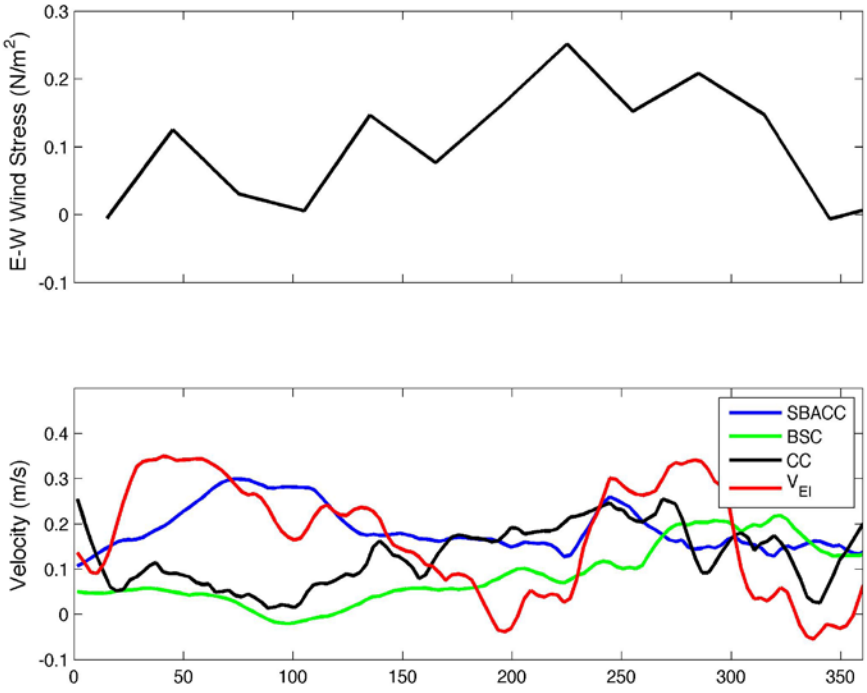

Figure 14. Top panel: E-W component of surface wind stress over the SSIs shelf in 2004. Bottom panel: ACC current (blue) at the KGI segment, Bransfield Current (green) at KGI segment, Antarctic coastal current (black) over the northwest Weddell Shelf, and off-shelf current velocity (red) at Shackleton Bank segment (60^{o}30′N, 54^{o}W) in 2004. The locations chosen for representing ACC, BSC, and CC see Figure 12. The averaging band for the offshelf transport velocity sees Figure 13.

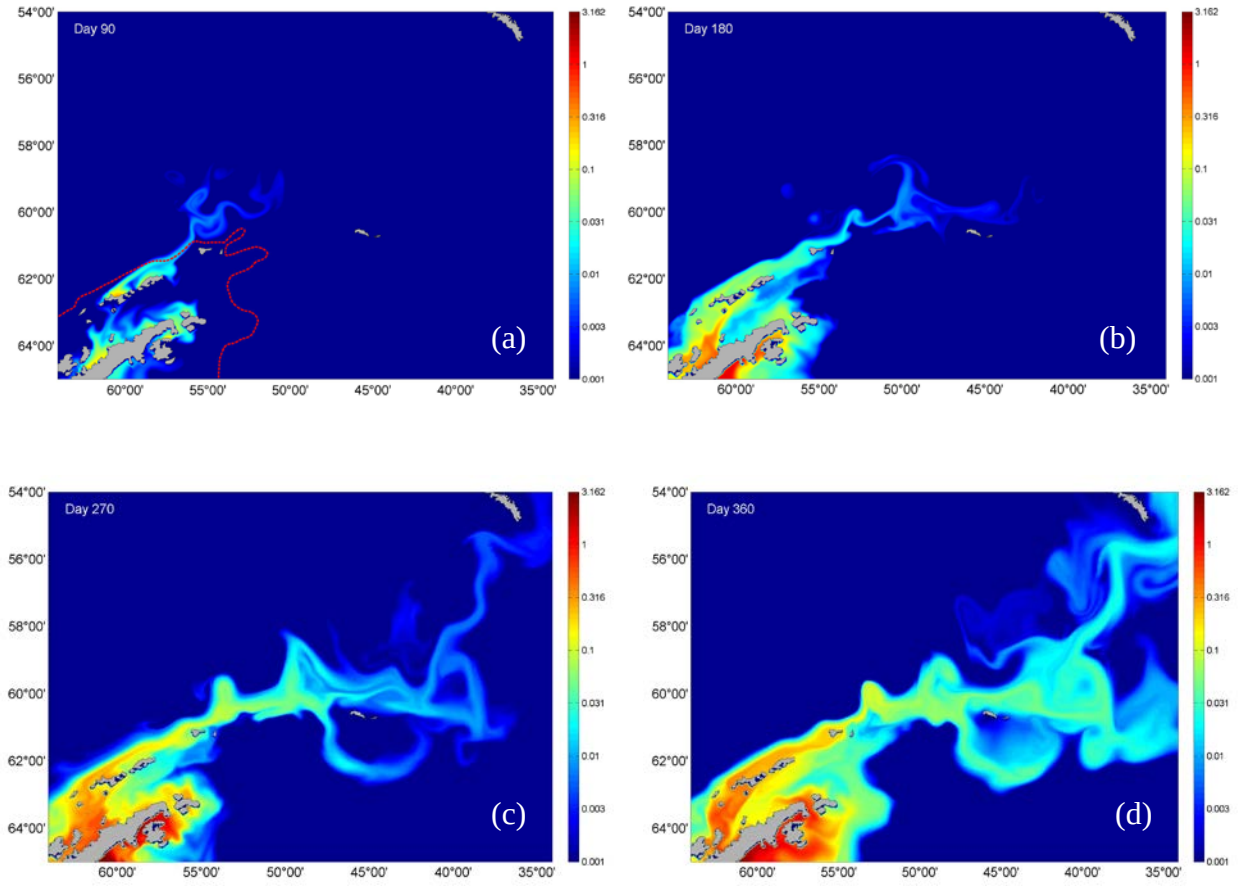

Figure 15. Snapshots of surface distributions of inert tracer continuously released from the sediment since January 1: (a) day 90, (b) day 180, (c) day 270 and (d) day 360. A uniform sediment flux of 1 TracerUnit*m/sec is applied to the bottom model layer of the Antarctic Peninsula region, which is defined as the area inside of 1000 m depth contour over the shelf slope (see red dashed contour in (a)).

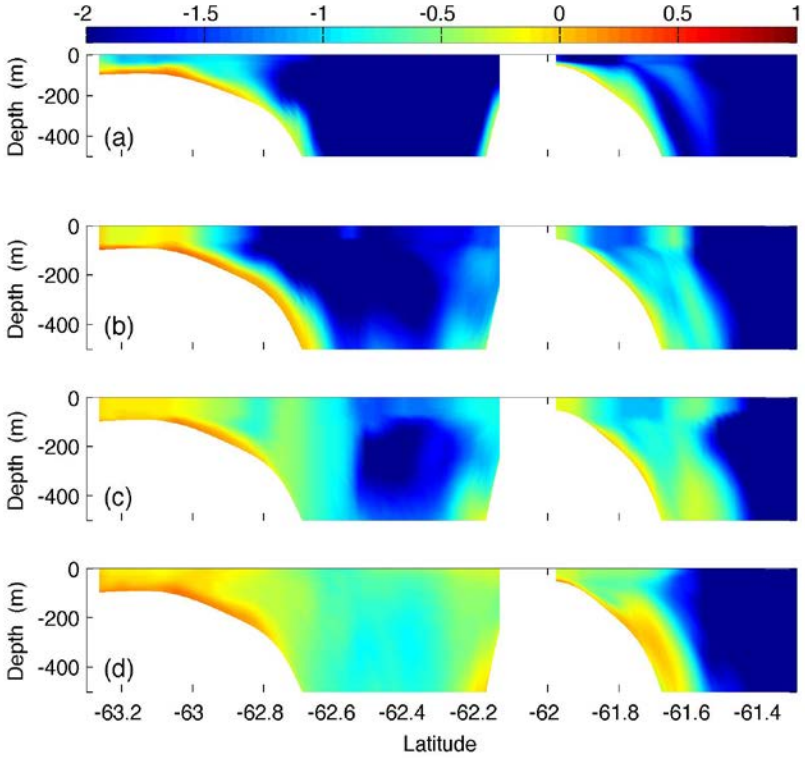

Figure 16. Monthly averaged distributions of the inert tracer (log10(Ra)) along BS transect crossing Bransfield Strait and SSIs shelf/slope (see Figure 1): (a) 3 months, (b) 6 months, (c) 9 months and (d) 12 months.